nature biotechnology

Generation of bispecific IgG antibodies by structure-based design of an orthogonal Fab interface

Steven M Lewis[1,4], Xiufeng Wu[2,4], Anna Pustilnik[2], Arlene Sereno[2], Flora Huang[2], Heather L Rick, Gurkan Guntas[1], Andrew Leaver-Fay[1], Eric M Smith[2], Carolyn Ho[2], Christophe Hansen-Estruch[2], Aaron K Chamberlain[2], Stephanie M Truhlar[2], Elaine M Conner, Shane Atwell[2], Brian Kuhlman[1,3] & Stephen J Demarest[2]

Robust generation of IgG bispecific antibodies has been a long-standing challenge. Existing methods require extensive engineering of each individual antibody, discovery of common light chains, or complex and laborious biochemical processing. Here we combine computational and rational design approaches with experimental structural validation to generate antibody heavy and light chains with orthogonal Fab interfaces. Parental monoclonal antibodies incorporating these interfaces, when simultaneously co-expressed, assemble into bispecific IgG with improved heavy chain–light chain pairing. Bispecific IgGs generated with this approach exhibit pharmacokinetic and other desirable properties of native IgG, but bind target antigens monovalently. As such, these bispecific reagents may be useful in many biotechnological applications.

Bispecific antibodies (BsAbs), which target two antigens or epitopes, incorporate the specificities and properties of two distinct monoclonal antibodies (mAbs) into a single molecule. As such, BsAbs can elicit synergistic activities such as co-clustering of signaling receptors or unique activities such as targeting immune cells to kill cancer cells. However, many existing BsAb formats have drawbacks. For example, some of the most common BsAb formats, such as diabodies, IgG-single-chain (sc) Fv and dual variable domain (DVD)-Ig[1], alter the native antibody geometry with its well-known stability and solubility properties to achieve specificity for multiple antigens. BsAb formats using antibody fragments (either domain antibodies, scFvs or diabodies) commonly require extensive engineering to stabilize the variable domains outside the native Fab context[2]. In addition, IgG-scFv and DVD-Ig BsAbs are tetravalent, whereas many clinical applications, such as T-cell-redirected tumor targeting or the inhibition of certain receptor tyrosine kinases (RTKs), require monovalent antigen recognition to avoid unwanted agonism[3,4].

Existing methods for producing native-like IgG BsAbs also have limitations. For example, IgG BsAbs have been produced by expressing mAbs separately[5,6] and then recombining them using protein engineering and biochemical methods, but this is time consuming and requires the generation of two master cell lines. Spiess *et al.* have generated IgG BsAbs by culturing two transformed *Escherichia coli* cell lines together[7], but ideally one would be able to produce the BsAb using a single cell line. The variable domains of IgGs can also be individually engineered to simultaneously recognize two antigens, but this method requires separate engineering for each antigen pair that is targeted[8].

Theoretically, one could assemble an IgG BsAb by coexpressing two parental mAbs. However, co-expressing two heavy chains and two light chains to generate an IgG BsAb generally results in some misassembly and by-products. For example, two heavy chains from the same parental mAb may pair with each other (forming heavy chain homodimers) rather than with the heavy chain from the other parental mAb. In addition, the heavy chain of one parental mAb may assemble with the light chain of the other parental mAb (**Fig. 1a**). To prevent formation of heavy chain homodimers, one could engineer a C_H3 domain that promotes heavy chain heterodimerization. In fact, the first solution to the C_H3 homodimerization/heterodimerization issue was described almost 20 years ago[9] and has been followed by other solutions that have been reviewed[10]. Solving the light chain mispairing problem is more difficult due to the complex multidomain heterodimeric interactions within antibody Fabs. One solution is to generate IgG BsAbs using a single light chain[11]; however, this requires light chain engineering or novel antibody libraries that utilize a single light chain, thus eliminating a great deal of diversity. Another approach would be to design an orthogonal heavy chain–light chain interface that allows each light chain to bind to its cognate heavy chain with higher affinity than the noncognate heavy chain. For example, one can swap the C_H1 domain of one heavy chain with the C_L domain of its cognate light chain[12]. However, we have found that V_H-V_L interactions can dominate the interaction specificities between heavy chains and light chains; this might complicate or over-ride any pairing specificity imparted by swapping constant domains between heavy chains and light chains. For these reasons, designing a fully orthogonal heavy chain–light chain interface may be a more robust solution for deriving the desired heavy chain–light chain specificity. Here, we describe the design of an orthogonal IgG heavy chain–light chain interface using molecular modeling, feedback from X-ray crystallography and human-guided design.

[1]Department of Biochemistry and Biophysics, University of North Carolina at Chapel Hill, Chapel Hill, North Carolina, USA. [2]Eli Lilly Biotechnology Center, San Diego, California, USA. [3]Lineberger Comprehensive Cancer Center, University of North Carolina at Chapel Hill, Chapel Hill, North Carolina, USA. [4]These authors contributed equally to this work. Correspondence should be addressed to B.K. (bkuhlman@email.unc.edu) or S.J.D. (demarestsj@lilly.com).

Received 1 July 2013; accepted 10 December 2013; published online 26 January 2014; doi:10.1038/nbt.2797

RESULTS

Design of an orthogonal C_H1-C_L interface

We focused our initial efforts on redesigning the C_H1-C_L interface. To generate a mutant C_H1-C_L interface that disfavors binding to wild-type (WT) C_H1-C_L, we used the multistate design application in the modeling program Rosetta[13]. During multistate design, candidate sequences are evaluated by building models of the target and off-target complexes, predicting the binding energies of the two complexes, and searching for mutations that increase the energy gap between the target and off-target interactions while maintaining the stability of the target complex[14–16]. By performing independent simulations focused on residue clusters in different regions of the interface, we identified 20 design paradigms predicted to favor mutant-mutant pairing over the mutant-WT pairs (**Supplementary Table 1**). We use 'design paradigm' to refer to a set of sequences that are highly similar and predicted to be iso-energetic. From the 20 design paradigms, more than 40 specific sequences were constructed and screened in the laboratory.

Experimentally evaluating the characteristics of the C_H1-C_L designs required generating an IgG1 construct lacking variable domains, denoted IgG1(–Fv) (**Supplementary Fig. 1**). The component proteins of IgG1(–Fv) assembled properly as revealed by SDS-PAGE analysis, and this complex was monodisperse with a molecular weight of 95 kDa, as shown by size-exclusion chromatography (SEC) with in-line static light scattering (SLS); it was highly stable as shown by differential scanning calorimetry (DSC) measurements (**Supplementary Fig. 1**).

Sequences from ten of the design paradigms were expressed at levels similar to that of the WT IgG1(–Fv) after transient transfection in human embryonic kidney (HEK)293F cells (**Supplementary Table 1**). In general, the designed proteins that were well expressed had fewer mutations, and all proteins with more than nine mutations were not expressed. Mutant proteins that were expressed robustly were further transfected as mismatched heavy chain–light chain pairs with WT heavy chain or light chain. Mutant proteins from three design paradigms had mutant-mutant pairs that were more stable than mismatched mutant-WT pairs. Each of these paradigms contained at most three mutations.

Two distinct designs, C_L_L135F/C_H1_V190F_F174T and C_L_K129D/C_H1_D146K (for sequence context see **Supplementary Fig. 2**) were marginally orthogonal on their own so we combined the mutations into a single combination design, denoted as constant redesign 1 or CRD1. Expression levels of the CRD1 C_H1-Cλ pair were 50% of WT, and its thermal unfolding temperature was near that of the WT pair (data not shown). We solved high-resolution crystal structures of the WT C_H1-Cλ heterodimer (PDB: 4LLD, 1.19 Å) and the CRD1 C_H1-Cλ heterodimer (PDB: 4LLM, 1.75 Å) (**Fig. 1b**,**c**). The crystal structure of the CRD1 heterodimer closely matches the Rosetta-based model, with 1.07 Å r.m.s. deviation over all nonhydrogen atoms in the three core repacked residues of CRD1 (**Fig. 1c**).

A third design denoted CRD2β (C_L_L135A_S176W/C_H1_F174G) also exhibited promising specificity and stability. The matched CRD2β heavy chain–CRD2β light chain pair was expressed better and was more stable than the mismatched pairs (WT light chain–CRD2β heavy chain and CRD2β light chain–WT heavy chain; data not shown). CRD2β was designed to introduce a severe steric clash with residues at the interior of the WT interface (**Fig. 1d**). However, the crystal structure of CRD2β (PDB: 4LLQ, 1.42 Å) showed a prolyl *trans-cis* peptide bond isomerization between C_H1_F174G and C_H1_P175 that allowed for the introduced tryptophan at Cλ_176 to flip orientations relative to the model (**Supplementary Fig. 3c**). We interpreted the mismatch between design and crystal structure to mean that the tryptophan was underpacked.

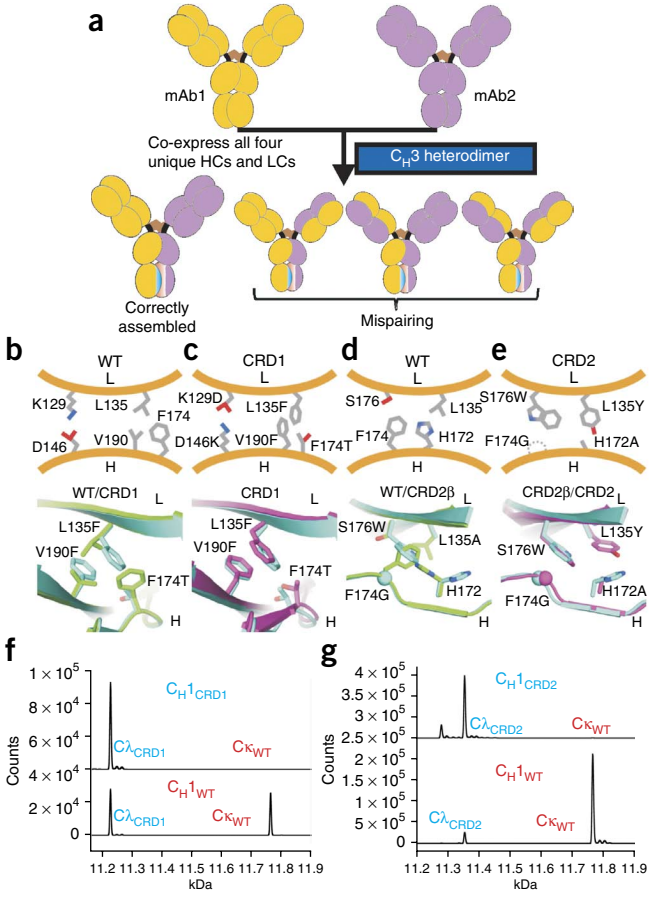

Figure 1 Design of an orthogonal C_H1-C_L interface. (**a**) Schematic diagram of possible by-products of IgG BsAb assembly. Top, heterotetrameric structures of two parental mAbs (mAb1 and mAb2) that hypothetically recognize different antigens. Each parental mAb consists of a unique heavy chain and a unique light chain. If both sets of heavy chain and light chain are transfected into the same cell for simultaneous expression, existing C_H3 heterodimer approaches can be used to encourage heterodimeric and discourage homodimeric heavy chain association. However, without engineering the heavy chain–light chain interface, each light chain can associate with the wrong heavy chain partner. As a result, three incorrectly assembled by-products can be generated. (**b**–**e**) Schematic diagrams, models and X-ray structures of designs CRD1 and CRD2. (**b**–**e**) Top row presents schematic diagrams of WT (**b**,**d**), CRD1 (**c**) and CRD2 (**e**) portions of the C_H1-C_L interface; mutations are indicated. Within each panel, the top portion represents C_L and the bottom, C_H1. Bottom row, overlays of the Rosetta-designed models and actual crystal structures. In **b**,**d**, crystal structures of the WT C_H1-C_L interface (3TV3) are in green and a Rosetta-designed orthogonal model cluster is shown in blue. In **c**,**e**, the models are in blue and the crystal structures are in magenta. The CRD1 structure at the bottom of **c** is from 4LLM, and CRD2 in **e** is from 4LLY. The structures in **b** and **c** omit K129(D) and D146(K), which are distal to the repacked core. (**f**,**g**) Competition assays where two light chain constant domains (WT and either CRD1 (**f**) or CRD2 (**g**)) were expressed with a single heavy chain and forced to compete for assembly. The deconvoluted mass spectra indicate the relative detector counts for $C\kappa_{WT}$ and $C\lambda_{CRD1}$ when expressed and co-purified with a heavy chain containing C_H1_{CRD1} (top) or C_H1_{WT} (bottom) (**f**) or $C\kappa_{WT}$ and $C\lambda_{CRD2}$ when expressed and co-purified with a heavy chain containing C_H1_{CRD2} (top) or C_H1_{WT} (bottom) (**g**). The competition assays were done at least three times on separate occasions. The average ratio of the peak areas is provided in **Supplementary Table 2**.

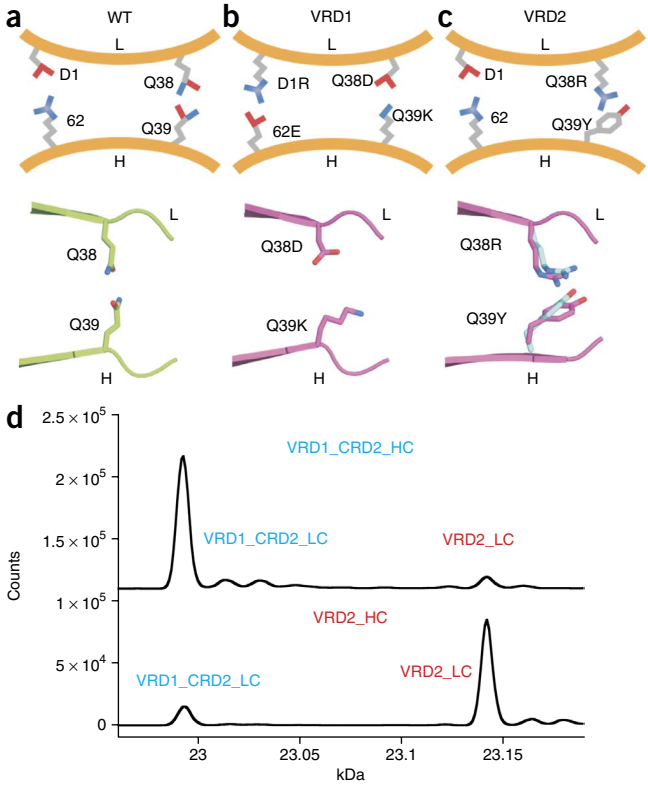

Figure 2 Schematic diagrams, models and X-ray structures of designs VRD1 and VRD2. (**a**–**c**) Top row, schematic diagrams of WT (**a**) VRD1 (**b**) and VRD2 (**c**) portions of the V_H1-V_L interface; mutations are indicated. Within each panel, the top portion represents V_L and the bottom V_H. The bottom of **a** shows, in green, V_L_Q38/V_H_Q39 from the WT pertuzumab Fab crystal structure 4LLU; the bottom of **b** shows the rationally designed VRD1 mutations (V_L_Q38D/V_H_Q39K) from a second Fab structure (4LLY); and the bottom of **c** shows VRD2 (V_L_Q38R/V_H_Q39Y) with the initial model in blue and the subsequent crystal structure (4LLW) in magenta. The blue design backbone is not shown, for clarity. (**d**) Competition assay where two light chain molecules (VRD1_CRD2_LC or VRD2_LC) are expressed with a single heavy chain (HC) and forced to compete for assembly. The deconvoluted mass spectra show the relative detector counts for VRD1_CRD2_LC and VRD2_LC when expressed and co-purified with VRD1_CRD2_HC (top) or VRD2_HC (bottom). The competition assays were done at least three times on separate occasions. The average ratio of the peak areas is provided in **Supplementary Table 2**.

We then performed a second round of multistate simulations, with the CRD2β structure as a starting point, to more tightly pack the area around Cλ_W176, while steering further from the WT structure. After screening eight new designs, we found the most stable and highly expressed design consisted of C_L_L135Y _S176W/C_H1_H172A_ F174G (**Supplementary Fig. 2**), denoted as CRD2. The IgG(–Fv) protein with CRD2 was expressed slightly better than the WT, and its mismatched pairs were expressed poorly and were a mix of assembled and unassembled protein (**Supplementary Fig. 3f**). The apparent stability of CRD2 was similar to that of WT in the thermal challenge assay, and its mismatched pairs were less stable (**Supplementary Fig. 3h**).

A crystal structure of CRD2 revealed a reversion of the backbone and side chain structure to a conformation close to that of the original CRD2β design model (PDB: 4LLY, 1.60 Å). The crystal structure (**Fig. 1e**) shows how the C_H1 mutations F174G and H172A make room for the small-to-large C_L mutations S176W and L135Y. An overlay of the model of CRD2β and the crystal structure of CRD2 showed that W176 now adopts the rotamer predicted in the CRD2β model and the peptide bond between residues 174 and 175 is in the native *trans* conformation with very little change in Fab structure outside the mutated regions (**Fig. 1e** and **Supplementary Fig. 4**).

Next, we performed a competition experiment in which two C_L (one WT and one mutant) were co-expressed with a single IgG(–Fv) heavy chain harboring a WT or mutant C_H1. Mass spectrometry (MS) was used to determine if the matched C_L outcompeted the mismatched C_L for IgG(–Fv) heavy chain association and secretion. $C\lambda_{CRD1}$ outcompeted $C\kappa_{WT}$ and $C\lambda_{WT}$ for binding to IgG(–Fv) harboring C_H1_{CRD1} (**Supplementary Table 2** and **Fig. 1f**). However, $C\lambda_{WT}$ and $C\kappa_{WT}$ bound to roughly the same extent as $C\lambda_{CRD1}$ did to the IgG(–Fv) harboring C_H1_{WT}. $C\lambda_{CRD2}$ outcompeted both $C\kappa_{WT}$ and $C\lambda_{WT}$ for binding IgG(–Fv) harboring C_H1_{CRD2} (100%), and $C\kappa_{WT}$ and $C\lambda_{WT}$ largely outcompeted $C\lambda_{CRD2}$ for binding to IgG(–Fv) heavy chain harboring C_H1_{WT} (95% and 93%, respectively; **Supplementary Table 2** and **Fig. 1g**). Based on these experiments, CRD2 was superior to CDR1 in terms of expression, stability and specificity.

The specificity afforded by CRD1 and CRD2 in the IgG(–Fv) format did not translate to the IgG format containing pertuzumab (Perjeta; breast cancer drug) V_H and V_L. When the same competition experiments described above for IgG(–Fv) were performed using full-length light chains and heavy chains containing WT and either CRD1 or CRD2 C_H1-C_L domains, pairing specificity was not observed (**Supplementary Table 2**). This loss of specificity was unexpected because C_H1-Cλ unfolds cooperatively with a high T_m of 78 °C, whereas the pertuzumab V_H and V_L in a similar scFv-Fc format unfold noncooperatively with T_m of 55 °C and 70 °C, respectively (**Supplementary Fig. 1d**). Therefore, we turned our efforts to designing additional pairing specificity within the V_H-V_L interface.

Design of an orthogonal V_H-V_L interface

The main objectives for the V_H-V_L interface redesign were (i) to modify conserved residues wherever possible to allow the solutions to be applicable across multiple V_H-V_L germline segments and (ii) to minimize the impact upon antigen binding. First, we rationally introduced charged residues at the highly conserved V_L_Q38-V_H_Q39 hydrogen bonded pair at the 'bottom' of the Fv, far removed from the complementarity determining regions (CDRs). Charge pairs were introduced into scFvs and diabodies at these positions previously without markedly altering Fv stability[17,18]. Among all possible charge-paired variants, the V_L_Q38D-V_H_Q39K pair was the most well-accommodated within the pertuzumab Fab, based on its expression level (data not shown). Next, we reversed the charge of the conserved V_L_D1 and added a negatively charged residue in V_H to facilitate additional specificity. The most well-expressed charge reversal was V_L_D1R and V_H_R62E (data not shown). The molecules encoding the two charge pairs (V_L_Q38D-V_H_Q39K/V_L_D1R-V_H_R62E) were denoted VRD1 (**Supplementary Fig. 2**). Crystal structures of the WT Fab (PDB: 4LLU, 2.16 Å) and a Fab containing VRD1 (PDB: 4LLY, 1.60 Å) showed that areas of the structure outside the mutated regions were unperturbed (**Fig. 2a**,**b** and **Supplementary Fig. 4**).

Multistate design used to generate other V_H-V_L interface designs coincidentally suggested other mutations at the same V_L_Q38-V_H_Q39 residue pair (**Supplementary Table 1**). Screening for expression and stability identified V_L_Q38R-V_H_Q39Y, denoted VRD2 (**Supplementary Fig. 2**), as a strong candidate for improving heavy chain–light chain specificity (**Fig. 2c**). A crystal structure of VRD2 showed that R38 and Y39 formed a cation-π interaction as modeled

Table 1 Accuracy of IgG BsAb assembly

IgG BsAb[a]	HC1[b] pertuzumab (–)	LC1 pertuzumab	HC2 matuzumab (+)	LC2 matuzumab	LC1 + LC2[c] (% correct)	$LC1_2$ (% not correct)	$LC2_2$ (% not correct)	Expression μg/ml
Anti-HER2 × Anti-EGFR IgG BsAbs (2 ml culture)								
HEControlλλ[c]	$VH_{WT}CH1_{WT}$	$VL_{WT}C\lambda_{WT}$	$VH_{WT}CH1_{WT}$	$VL_{WT}C\lambda_{WT}$	65 ± 2	24 ± 4	11 ± 3	25 ± 8
HEControlλκ	$VH_{WT}CH1_{WT}$	$VL_{WT}C\lambda_{WT}$	$VH_{WT}CH1_{WT}$	$VL_{WT}C\kappa_{WT}$	75 ± 1	13 ± 6	12 ± 6	42 ± 23
HEDesignλλ	$VH_{VRD1}CH1_{CRD2}$	$VL_{VRD1}C\lambda_{CRD2}$	$VH_{VRD2}CH1_{WT}$	$VL_{VRD2}C\lambda_{WT}$	93 ± 5	6 ± 4	2 ± 2	34 ± 15
HEDesignλκ	$VH_{VRD1}CH1_{CRD2}$	$VL_{VRD1}C\lambda_{CRD2}$	$VH_{VRD2}CH1_{WT}$	$VL_{VRD2}C\kappa_{WT}$	93 ± 4	4 ± 3	3 ± 3	34 ± 19
Anti-cMET × Anti-Axl IgG BsAbs (2 ml culture)								
IgG BsAb	HC1 MetMAb (–)	LC1 MetMAb	HC2 anti-Axl (+)	LC2 anti-Axl				
MAControlλλ	$VH_{WT}CH1_{WT}$	$VL_{WT}C\lambda_{WT}$	$VH_{WT}CH1_{WT}$	$VL_{WT}C\lambda_{WT}$	64 ± 19	29 ± 24	7 ± 7	58 ± 25
MAControlλκ	$VH_{WT}CH1_{WT}$	$VL_{WT}C\lambda_{WT}$	$VH_{WT}CH1_{WT}$	$VL_{WT}C\kappa_{WT}$	59 ± 3	35 ± 11	7 ± 11	15 ± 13
MADesignλλ	$VH_{VRD1}CH1_{CRD2}$	$VL_{VRD1}C\lambda_{CRD2}$	$VH_{VRD2}CH1_{WT}$	$VL_{VRD2}C\lambda_{WT}$	90 ± 9	1 ± 1	9 ± 9	44 ± 18
MADesignλκ	$VH_{VRD1}CH1_{CRD2}$	$VL_{VRD1}C\lambda_{CRD2}$	$VH_{VRD2}CH1_{WT}$	$VL_{VRD2}C\kappa_{WT}$	88 ± 10	0	12 ± 10	71 ± 6
Other IgG BsAbs (2 ml culture)								
EGFR × cMETλλ	Matuzumab $VH_{VRD2}CH1_{WT}$	Matuzumab $VL_{VRD2}C\lambda_{WT}$	MetMAb $VH_{VRD1}CH1_{CRD2}$	MetMAb $VL_{VRD1}C\lambda_{CRD2}$	93 ± 6	0	7 ± 6	12 ± 2
EGFR × LTβRλλ	Matuzumab $VH_{VRD1}CH1_{CRD2}$	Matuzumab $VL_{VRD1}C\lambda_{CRD2}$	BHA10 $VH_{VRD2}CH1_{WT}$	BHA10 $VL_{VRD2}C\lambda_{WT}$	95 ± 3	5 ± 3	0	56 ± 7
$HER2^P$× $HER2^T$κκ	Pertuzumab $VH_{VRD2}CH1_{WT}$	Pertuzumab $VL_{VRD2}C\kappa_{WT}$	Trastuzumab $VH_{VRD1}CH1_{CRD2}$	Trastuzumab $VL_{VRD1}C\kappa_{CRD2}$	100 ± 0	0	0	68 ± 12
IgG BsAbs (1 liter culture)								
HER2 × EGFRλλ	Pertuzumab $VH_{VRD1}CH1_{CRD2}$	Pertuzumab $VL_{VRD1}C\lambda_{CRD2}$	Matuzumab $VH_{VRD2}CH1_{WT}$	Matuzumab $VL_{VRD2}C\lambda_{WT}$	90	5	5	52
cMETxAxlλλ	MetMAb $VH_{VRD1}CH1_{CRD2}$	MetMAb $VL_{VRD1}C\lambda_{CRD2}$	Anti-Axl $VH_{VRD2}CH1_{WT}$	Anti-Axl $VL_{VRD2}C\lambda_{WT}$	95	3	2	25
EGFR × cMETλλ	Matuzumab $VH_{VRD2}CH1_{WT}$	Matuzumab $VL_{VRD2}C\lambda_{WT}$	MetMAb $VH_{VRD1}CH1_{CRD2}$	MetMAb $VL_{VRD1}C\lambda_{CRD2}$	94 ± 2	1 ± 2	5 ± 3	28 ± 28
$HER2^P$ × $HER2^T$κκ	Pertuzumab $VH_{VRD2}CH1_{WT}$	Pertuzumab $VL_{VRD2}C\kappa_{WT}$	Trastuzumab $VH_{VRD1}CH1_{CRD2}$	Trastuzumab $VL_{VRD1}C\kappa_{CRD2}$	100 ± 0	0	0	72 ± 9

All values in **Table 1** that include s.d. were derived from three or more independent measurements.
[a]Each BsAb is designated as 'HE' or 'MA' to denote HER2 × EGFR or cMet × Axl, respectively; 'control' denotes the absence of the Fab designs described here; λλ,κκ, and λκ denote the C_L compositions of the two light chains. [b]The pertuzumab and MetMAb heavy chains have the negatively charged half of the C_H3 heterodimer design '(–)' and the matuzumab and anti-Axl heavy chains have the positively charged half of the C_H3 heterodimer design '(+)'. [c]The LC/MS method can detect heterotetrameric IgGs containing mismatched heavy chain pairs (HC1 or HC2), but none were detected. The percent values represent the percent of the detector counts detected for correctly covalently linked heterotetramers heavy chain1-heavy chain2-light chain1-light chain2 (LC1 + LC2) compared with incorrectly formed heavy chain1-heavy chain2-light chain1-light chain1 ($LC1_2$) and heavy chain1-heavy chain2-light chain2-light chain2 ($LC2_2$) heterotetramers.

with very little change to the WT Fab outside the mutated regions (**Fig. 2c** and **Supplementary Fig. 4**; PDB: 4LLW, 1.95 Å).

Next we screened the variable domain designs by light chain competition for binding to specific heavy chains. All heavy chains and light chains, both designed and WT, contained pertuzumab V_H and V_L, respectively. First, we co-expressed VRD1 or VRD2 light chain together with the WT light chain and a single heavy chain. Relative to WT light chain, both VRD1 and VRD2 bound more efficiently to their cognate mutant heavy chain and less efficiently to WT heavy chain; however, in some cases the degree of orthogonality was modest (**Supplementary Table 2**). Increased orthogonality was achieved when the VRD1 and VRD2 light chains competed against one another (rather than against WT light chain) for binding to either a VRD1 heavy chain or VRD2 heavy chain (**Supplementary Table 2**).

Next, we tested the impact of combining VRD1 and VRD2 with CRD2. Adding CRD2 to either VRD1 or VRD2 boosted the observed specificity of both VRD1 light chain and VRD2 light chain for binding to VRD1 or VRD2 heavy chains, respectively, in the competition assay. However, both VRD1_CRD2 light chain and VRD2_CRD2 light chain still paired relatively frequently with WT heavy chain (**Supplementary Table 2**). Therefore, we tested VRD1_CRD2 light chain against VRD2 light chain for binding VRD1_CRD2 heavy chain or VRD2 heavy chain; in this scenario we observed 87% and 91% specificity, respectively (**Fig. 2d** and **Supplementary Table 2**). We hypothesize that the V_H_VRD1 mutant Q39K clashes strongly with V_L_VRD2 mutant Q38R, resulting in significantly improved specificity over combinations involving WT chains.

We produced IgG1 proteins containing VRD1_CRD2 or VRD2 by transient expression in HEK293F cells and purified them using a single-step protein A column. Both VRD1_CRD2 and VRD2 IgGs were monomeric as shown by SEC-SLS (**Supplementary Fig. 5a**). The IgGs had Fab T_ms of 71 °C and 73 °C, respectively, comparable to the WT pertuzumab Fab T_m (77 °C) and higher than the first unfolding event (T_m = 55 °C) of an scFv derived from pertuzumab (**Supplementary Fig. 5b**). Moreover, the HER2 antigen binding kinetics of the designed Fabs were identical to those of the WT pertuzumab Fab (**Supplementary Fig. 5c**).

Our method requires the introduction of multiple mutations into conserved framework regions of both variable and constant domains. It thereby has the potential to generate new B- and T-cell epitopes and undesired anti-drug antibody responses in humans. Initial prediction of T-cell epitopes using the EpiVax server indicated no increase of immunogenicity (**Supplementary Table 3**)[19]. However, further studies with therapeutic candidate molecules will be required to adequately assess this question.

Generation of bispecific IgGs

To test the feasibility of producing IgG BsAbs using the designed mutant Fabs, we assembled five different IgG1 BsAbs using six parental IgG1 mAbs. The first BsAb, HER2 × EGFR, paired pertuzumab and matuzumab (an anti-EGFR mAb)[20,21]; the second, cMet × Axl, paired anti-cMet mAb (MetMAb) and the anti-Axl IgG1 YW327.6S2 (refs. 4,22); the third, EGFR × cMet, paired matuzumab and MetMAb; the fourth, EGFR × LTβR, paired matuzumab and the

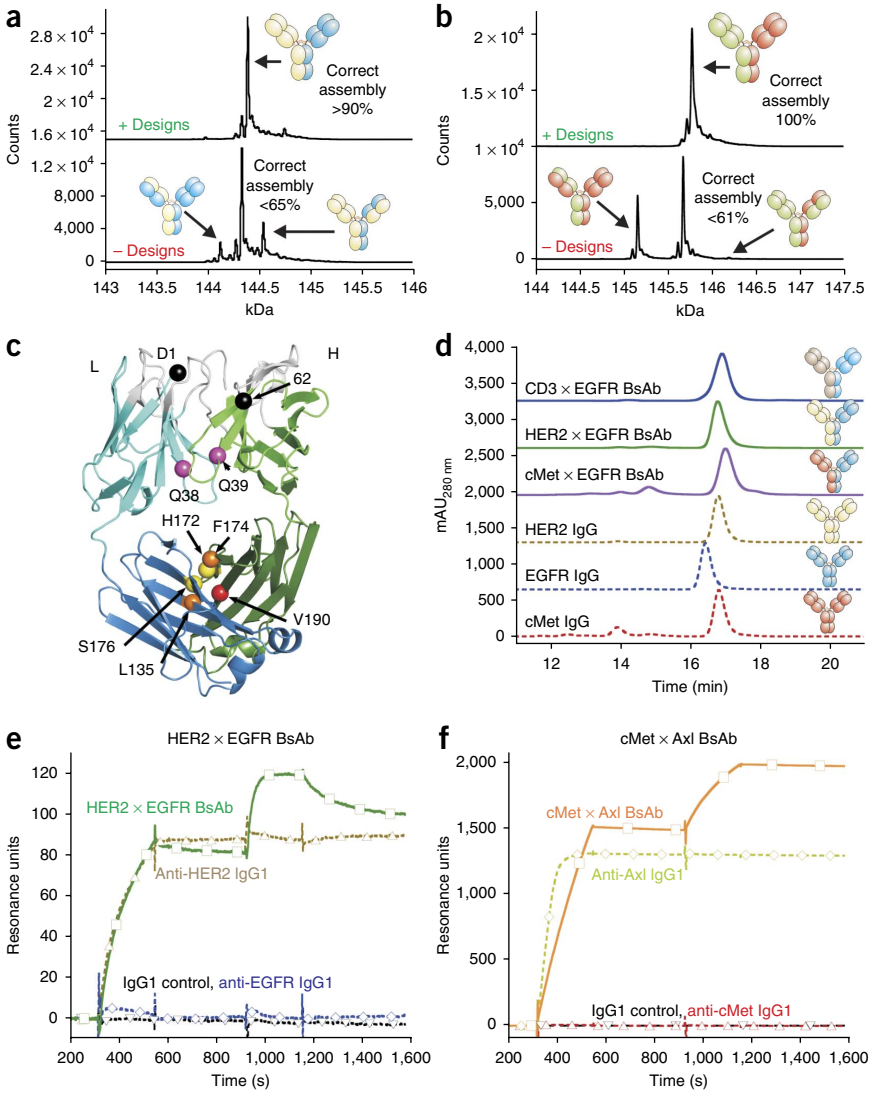

Figure 3 Demonstration of the specificity afforded by the heavy chain–light chain interface designed mutants and the dual-binding activity of the resulting BsAb molecules. (**a**) Deconvoluted mass spectra of the assembled heterotetrameric HER2 × EGFR IgG1 proteins (lacking glycosylation) using a published C_H3 heterodimer mechanism[24] in the absence (bottom) and presence (top) of the heavy chain–light chain interface designs (VRD1_CRD2 in one heavy chain–light chain set and VRD2 in the other). (**b**) The same analysis as in **a** using a different set of parental mAbs to generate cMet × Axl IgG BsAbs. Peak area results of at least three independent replicates of **a** and **b** are provided in **Table 1**. (**c**) Ribbon diagram of the pertuzumab Fab structure showing the location of the mutations (highlighted as spheres) within CRD1, CRD2, VRD1 and VRD2. The light chain is on the left in blue, and the heavy chain is on the right in green. The CDR loops are in white at the top, the Fv is in lighter colors toward the top and C_L and C_H1 are in darker colors toward the bottom. Black spheres show positions mutated in VRD1. Magenta spheres show positions mutated in both VRD1 and VRD2. Orange spheres show positions mutated in both CRD1 and CRD2. Yellow spheres show positions mutated only in CRD2. The red sphere shows the single position mutated only in CRD1. (**d**) Single analytical SEC runs of the parental (monospecific) cMet, EGFR and HER2 IgG1 mAbs and cMet × EGFR, HER2 × EGFR and CD3 × EGFR IgG1 BsAbs after one-step protein A purification. (**e**,**f**) Dual antigen binding behavior of the HER2 × EGFR IgG1 BsAb (**e**) and the cMet × Axl IgG1 BsAb (**f**), as demonstrated using surface plasmon resonance (single experiment). The HER2 × EGFR BsAb was injected over a surface containing immobilized HER2 antigen (300–540 s) followed by injection of EGFR-Fc (920–1160 s). The controls were anti-HER2 IgG1 (pertuzumab), anti-EGFR IgG1 (matuzumab) and nonspecific IgG1. The cMet × Axl IgG1 BsAb was injected over a surface containing immobilized Axl antigen followed by injection of cMet-Fc. The controls were anti-Axl IgG1, two-arm anti-cMet IgG1 and a nonspecific IgG1 control.

anti-LTβR IgG BHA10 (ref. 23); the fifth, $HER2^P \times HER2^T$, paired pertuzumab and trastuzumab (Herceptin; for HER2-positive metastatic breast cancer), which recognize two different epitopes on HER2 (ref. 20). To induce heavy chain heterodimerization, we inserted previously described mutations into the C_H3 domains of each pair of parental mAbs[24]. The universal *N*-linked glycosylation site was mutated (N297Q) in most of the pairs to simplify MS analyses. For the HER2 × EGFR and cMet × Axl BsAbs, each light chain was built with both Cκ and Cλ to evaluate the impact of the C_L isotype on the Fab designs. As a control to assess the impact of the Fab designs on the correct heavy chain–light chain assembly, the HER2 × EGFR and cMet × Axl IgG BsAbs were also produced in the absence of Fab designs, but with the heterodimeric C_H3. The amino acid sequences of each heavy chain and light chain used to produce the IgG BsAbs, including the design mutations, are provided in **Supplementary Figure 6**.

Each of the mAb pairs (two heavy chains and two light chains) was transfected into a 2-ml culture of HEK293F cells. After protein G purification, the IgG BsAbs with and without Fab designs were subjected to MS analysis. All transfections were performed in triplicate (at least) on different days and the averages and s.d. of the assembly as determined by MS are listed in **Table 1**. In the absence of Fab specificity designs, the average correct assembly for the HER2 × EGFR and cMet × Axl BsAbs was 70% and 61%, respectively, which was higher than the 50% expected if each light chain had a similar affinity toward each heavy chain (**Fig. 3a**,**b** and **Table 1**). This may be explained by the natural complementarity of CDR pairing within individual mAbs. The MS technique could not differentiate between a correctly assembled IgG BsAb and an IgG with both light chains mispaired; however, as the level of single light chain mispairing decreases, the likelihood of both light chains mispairing becomes negligible. Adding the Fab designs increased the percent of correctly assembled IgG BsAbs to an average of 93% (with the Fab designed mutations, correct assembly ranged from 88% to 100%; **Fig. 3a**,**b** and **Table 1**). All the BsAbs, except $HER2^P \times HER2^T$, were built with Cλ in VRD1_CRD2. We observed better assembly using the VRD1_CRD2 designs with Cλ over Cκ. For the $HER2^P \times HER2^T$ pair, the trastuzumab V_H-V_L interface was extraordinarily strong and necessitated an additional V_L mutation (Y36F), which is a naturally occurring germline variant, to temper the V_H-V_L affinity and keep the trastuzumab light chain from pairing with both sides (see **Supplementary Fig. 6** for the

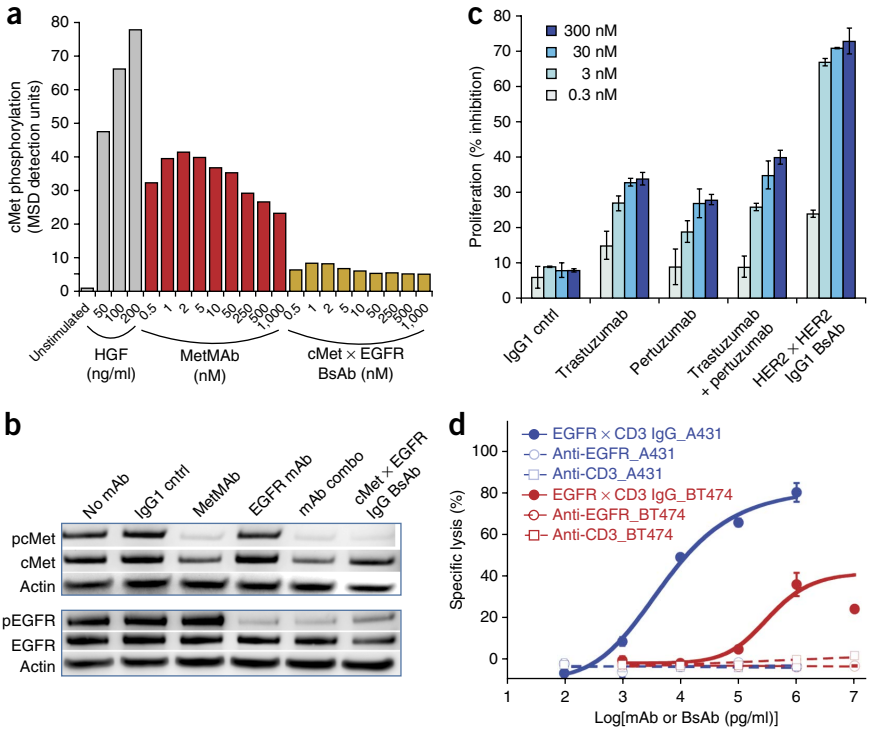

Figure 4 Function of IgG BsAbs. (**a**) A549 NSCLC cells were treated with the indicated concentrations of HGF, bivalent MetMAb or the cMet × EGFR IgG BsAb, or were left unstimulated. Phosphorylation of cMet was measured once per HGF/mAb/BsAb concentration using an anti-phospho-cMet capture/anti-cMet protein detection reagent system that elicits an electrochemiluminescent MSD signal. (**b**) A549 cells were treated with HGF and EGF, together with no mAb, IgG1 isotype control mAb, c-Met or EGFR-specific mAbs individually or together (combo), or with the cMet × EGFR IgG BsAb. Abundance of phosphorylated (pcMet, pEGFR) and total cMet and EGFR was measured by western blot analysis, with actin as the loading control. All experiments were performed once under serum-starved conditions. (**c**) N87 cells were incubated with FBS and various concentrations of the indicated antibodies. FBS-driven proliferation was measured by the Cell-Titer Glo reagent (Promega). At saturation, the IgG BsAb resulted in significantly more ($P < 0.001$) inhibition than did the mAb combo and individual mAbs based on a *t*-test comparing the different groups. (**d**) T-cell-redirected lysis of A431 (EGFR high) and BT474 (EGFR low) tumor cells by the EGFR × CD3 IgG BsAb. T cells were derived from human donor peripheral blood mononuclear cells (PBMCs) stimulated every few days with anti-CD3, anti-CD28 and interleukin-2. After 2 weeks of stimulation, the cell populations were consistently split between $CD4^+$ and $CD8^+$ T cells. The T cells were added at a 25:1 effector/tumor cell ratio. The extent of mAb- or BsAb-mediated specific lysis after 4 h of effector/tumor cell incubation was detected using the DELFIA tumor lysis assay. Error bars indicate s.d. of three independent measurements per data point for **c** and **d**.

sequence). This strategy has worked well with other pairings we tested in-house where strong V_H-V_L pairing precluded proper assembly. A ribbon diagram shows the locations of the VRD1, VRD2, CRD1 and CRD2 mutations within the Fab structure (**Fig. 3c**).

The thermal stability of the Fab regions of the mAbs in this study were assessed by DSC and they had T_ms ranging from 74–84 °C, which places these mAbs in the mid-to-high range for what has been observed for human or humanized mAbs ($68 < T_m < 82$ °C)[25]. In nearly all cases, one parental heavy chain–light chain pair was expressed at a higher level than the other parental heavy chain–light chain pair, resulting in a single heavy chain–light chain pair that was not covalently heterodimerized through the Fc; we refer to this as a "half-antibody." Half-antibody can be observed under denaturing conditions using SDS-PAGE or MS. In nearly all cases, the level of half-antibody could be controlled by transfecting a higher ratio of the more weakly expressed parental heavy chain–light chain pair (**Supplementary Fig. 7**). The degree of correctly assembled heavy chain–light chain pairing was not markedly affected by varying the transfection ratio of each parental heavy chain–light chain pair (**Supplementary Fig. 7**).

Next, we used the same plasmids encoding components of HER2 × EGFR, cMet × Axl, EGFR × cMet and $HER2^P$ × $HER2^T$ IgG BsAbs to produce the BsAbs in a 1-liter culture of HEK293F cells. The IgG BsAbs assembled with a nearly identical level of correct assembly as observed in the 2 ml transfections (**Table 1**). The EGFR × cMet and $HER2^P$ × $HER2^T$ transfections were performed in triplicate on different weeks. The average IgG BsAb titer was 44 mg/liter and within the range of expression we commonly observe for standard (monospecific) IgGs. The IgG BsAbs were predominately monomeric after protein G purification, similar to the parental mAbs (**Fig. 3d** and **Supplementary Fig. 8a**). The BsAbs assembled with very few by-products other than a small percentage of half-antibody (**Supplementary Fig. 8b–d**). DSC analysis indicated that the thermal stability of the $HER2^P$ × $HER2^T$ IgG BsAb is in the range commonly observed for mAbs[25]. The EGFR × cMet IgG BsAb had a lower (but acceptable) Fab T_m of 62 °C, which we believe is the result of pairing Vκ with Cλ (**Supplementary Fig. 8e,f**). The BsAbs were concentrated to >20 mg/ml in PBS without protein loss, insolubility or the accumulation of soluble aggregates. The BsAbs were digested with papain to liberate the Fab regions, and MS results of the digestion showed a similar level of correct heavy chain–light chain assembly as determined by intact mass analysis (**Supplementary Fig. 9a,d**). Whereas the proof-of-principle kinetic studies in **Figure 3e,f** demonstrate bispecific antigen binding, the solution-based antigen binding experiments in **Supplementary Figure 9b,c,e,f** show clearly that the EGFR × cMet and $HER2^P$ × $HER2^T$ IgG BsAbs bound monovalently to their target epitopes. Lastly, we analyzed *in vivo* pharmacokinetic parameters of the HER2 × EGFR and EGFR × cMet BsAbs, together with their parental mAbs, in male BALB/c mice. The HER2 × EGFR and EGFR × cMet BsAbs displayed pharmacokinetic parameters consistent with those of their parental mAbs (**Supplementary Fig. 10**).

Applications of bispecific IgGs

Finally, we used these new BsAbs in several biologically relevant applications. First, we used the EGFR × cMet BsAb to inhibit RTK activity. Because of their bivalent nature and tendency to cross-link cell surface receptors, many mAbs designed for the purpose of inhibiting ligand-mediated RTK phosphorylation instead exhibit intrinsic agonistic behavior resulting in receptor phosphorylation and internalization. An IgG BsAb that binds two receptors, each monovalently, may reduce receptor cross-linking. This was what we observed with the cMet × EGFR IgG BsAb designed here; it demonstrated markedly weaker overall agonism of cMet in A549 non–small cell lung carcinoma cells

(NSCLC) compared to a bivalent variant of MetMAb (**Fig. 4a**). The cMet × EGFR IgG BsAb also inhibited both HGF- and EGF-mediated receptor phosphorylation (**Fig. 4b**). Note that although the bivalent MetMAb appeared to be less agonistic in the western blot analysis than in the plate-based MSD immunoassay, this may be because we probed pTyr1234 in the western blot as opposed to overall pTyr in the MSD assay. Thus, the cMet × EGFR IgG reduced receptor agonism compared with the parental mAbs and still maintained the ability to block ligand-mediated receptor signaling. Interestingly, another report was recently published describing a separate strategy for generating a cMet × EGFR IgG BsAb by co-culturing two separate bacterial transformants, each containing half of the IgG BsAb[7].

Next, we assessed the ability of the $HER2^P \times HER2^T$ IgG BsAb to reduce serum-induced proliferation of HER2-positive N87 gastric cancer cells *in vitro* compared with the parental anti-HER2 mAbs trastuzumab and pertuzumab, which recently gained US Food and Drug Administration approval for use in combination in metastatic breast cancer[20]. The IgG BsAb induced significantly stronger growth inhibition compared with the single or combined parental mAbs ($P < 0.001$; **Fig. 4c**). The BsAb induced a greater accumulation of cPARP, a common hallmark of cellular apoptosis (data not shown). Although the molecular mechanism for the improved growth inhibition by the BsAb remains unclear, recent reports demonstrate that changing the geometry of HER2 engagement can have a considerable impact on the ability of a BsAb to kill tumor cells[26,27].

Lastly, we constructed a CD3 × EGFR IgG BsAb to redirect T cells to kill tumor cells[3]. To induce redirected tumor cell lysis, typically the T-cell-receptor–associated CD3ε component on T cells is engaged with one arm of a BsAb, whereas the other arm engages a tumor-specific antigen. Preferably, BsAbs bind each target monovalently, thereby avoiding generalized T-cell activation. Dual Fv formats, such as the bispecific T-cell engagers (BiTEs) and dual affinity retargeting bispecifics (DARTs)[3], are currently the leading BsAb platforms for T-cell-redirected tumor cell lysis. They face potential drawbacks, though, such as rapid clearance and in some cases manufacturing issues related to the non-native Fv format. The EGFR × CD3 IgG BsAb was expressed in HEK293F cells, purified using a single protein G step, and shown to be monomeric by SEC-SLS (**Fig. 3d**). Using flow cytometry, we evaluated several tumor cell lines for EGFR expression and chose A431 (160,000 receptors per cell) and BT474 (~2,000 receptors per cell) for their relatively high and low EGFR expression. Picomolar levels of the EGFR × CD3 IgG BsAb enabled T cells to kill 'EGFR high' A431 tumor cells, whereas approximately three orders of magnitude more BsAb was necessary to enable the killing of the 'EGFR low' BT474 cells, suggesting the potential for a therapeutic window using this approach on tumor cells overexpressing antigen (**Fig. 4d**).

DISCUSSION

Considering the significantly lower thermal stability and lack of cooperative unfolding of the V_H and V_L domains compared with the C_H1 and C_L domains (**Supplementary Fig. 1**), it was surprising that the variable domains dominated the specific assembly of heavy chains and light chains. The molecular basis for this dominance is not clear, although we speculate that it may be related to the kinetics of intracellular heavy and light chain association. The C_H1 domain is intrinsically unfolded in the absence of C_L and binds to the molecular chaperone BiP[28]. Only when the heavy chain engages the light chain can C_H1 be released from BiP to allow a fully assembled IgG molecule to be secreted[28]. It is possible that the folded V_H and V_L domains, although lower in apparent affinity, recognize one another first and drive the C_L domain to interact with unfolded C_H1 bound to BiP. If this variable domain dominance is a generalized phenomenon, it could present challenges for the crossover approach of swapping the V_H and V_L or C_H1 and C_L domains of the Fab between heavy chains and light chains[12]. Additionally, in cases where strong differences exist between V_H-V_L affinity of the parental mAbs being combined, as with the trastuzumab and pertuzumab pair, a slight rebalancing of the V_H-V_L affinity may be necessary to achieve correct assembly.

Although our approach of combining the orthogonal heavy chain–light chain interface designs with the C_H3 domain heterodimer strategy[24] facilitated expression of correctly assembled IgG BsAbs using all parental mAbs studied here, further work is needed to determine if this strategy will be applicable to all antibodies. For example, as all of the heavy chains used to create IgG BsAbs in this study were derived from either V_H3 or V_H1 family germline segments, and all V_L domains were germline Vκ1 segments, it is not certain that this approach can be effectively generalized to antibodies incorporating other V_H or V_L family germline segments. However, based on sequence similarity, we believe the designs should be transferable to other germline families. That said, the VRD1 design is unlikely to work as robustly in Vλ as in Vκ because Vλ germline segments lack the N-terminal acidic residue that is swapped to a positively charged residue in VRD1. In addition, the parental mAbs used here were all of moderate to high thermal stability. It is likely that mAbs with poor stability may prove problematic for IgG BsAb assembly. Additionally, we found that CRD1 provides improved specificity using Cλ over Cκ, which may be an important consideration when generating IgG BsAbs using the novel Fab designs described here. Additional work is also needed to determine if this approach can be scaled up for industrial IgG BsAb production. Generating stably selected mammalian cell lines will be the next step in this process.

The IgG BsAb format designed here incorporates many desirable features including the biophysical behavior and pharmacokinetic properties of native IgG and the ability to facilitate monovalent antigen engagement in scenarios where bivalency can lead to unwanted activity. Thus, this approach holds the potential to generate robust therapeutics for the effective treatment of complex, multifaceted diseases.

METHODS

Methods and any associated references are available in the online version of the paper.

Accession codes. Structural data and coordinates for the WT C_H1-C_λ (4LLD), CRD1 C_H1-C_λ (4LLM), CRD2β C_H1-C_λ (4LLQ), WT pertuzumab Fab(with C_λ) (4LLU), VRD2 Fab (4LLW), and VRD1_CRD2 Fab (4LLY) have been deposited in the PDB. (See **Supplementary Table 4** for the statistics describing the structure determination.)

Note: Any Supplementary Information and Source Data files are available in the online version of the paper.

ACKNOWLEDGMENTS

This work was supported by the Lilly Research Laboratories and the Lilly Research Award Program (LRAP). We thank J. Hannah and B. Gutierrez for their help with transient transfection, R. Yuan and D. He for assistance with protein purification, M. Batt and J. Fitchett for their training and up keep of the mass spectrometry facility at Lilly. B. Stranges provided suggestions for the computational docking protocol. Use of the Advanced Photon Source, an Office of Science User Facility operated for the US Department of Energy (DOE) Office of Science by Argonne National Laboratory, was supported by the US DOE under Contract No. DE-AC02-06CH11357. Use of the Lilly Research Laboratories Collaborative Access Team (LRL-CAT) beamline at Sector 31 of the Advanced Photon Source was provided by

Eli Lilly Company, which operates the facility. We thank S. Wasserman, S. Sojitra, J. Koss for data collection and operation of the beamline.

AUTHOR CONTRIBUTIONS

All authors contributed to the concepts of the study. S.M.L. and B.K. performed the computational design, with advice from A.L.-F. B.K., A.K.C., S.M.T., S.M.L., S.J.D. and X.W. contributed to the rational designs. X.W., A.S., H.L.R., E.M.C., E.M.S., G.G., C.H., F.H., C.H.-E. and S.J.D. performed the experimental work. A.P. and S.A. performed the crystallization and structure determinations. B.K. and S.J.D. conceived the project. Writing of the paper was done in close collaboration by B.K., S.A., S.M.L. and S.J.D.

COMPETING FINANCIAL INTERESTS

The authors declare competing financial interests: details are available in the online version of the paper.

1. Chames, P. & Baty, D. Bispecific antibodies for cancer therapy: the light at the end of the tunnel? *mAbs* **1**, 539–547 (2009).
2. Demarest, S.J. & Glaser, S.M. Antibody therapeutics, antibody engineering, and the merits of protein stability. *Curr. Opin. Drug Discov. Devel.* **11**, 675–687 (2008).
3. Lum, L.G. & Thakur, A. Targeting T cells with bispecific antibodies for cancer therapy. *BioDrugs* **25**, 365–379 (2011).
4. Jin, H. *et al.* MetMAb, the one-armed 5D5 anti-c-Met antibody, inhibits orthotopic pancreatic tumor growth and improves survival. *Cancer Res.* **68**, 4360–4368 (2008).
5. Strop, P. *et al.* Generating bispecific human IgG1 and IgG2 antibodies from any antibody pair. *J. Mol. Biol.* **420**, 204–219 (2012).
6. Labrijn, A.F. *et al.* Efficient generation of stable bispecific IgG1 by controlled Fab-arm exchange. *Proc. Natl. Acad. Sci. USA* **110**, 5145–5150 (2013).
7. Spiess, C. *et al.* Bispecific antibodies with natural architecture produced by co-culture of bacteria expressing two distinct half-antibodies. *Nat. Biotechnol.* **31**, 753–758 (2013).
8. Bostrom, J. *et al.* Variants of the antibody herceptin that interact with HER2 and VEGF at the antigen binding site. *Science* **323**, 1610–1614 (2009).
9. Ridgway, J.B., Presta, L.G. & Carter, P. 'Knobs-into-holes' engineering of antibody CH3 domains for heavy chain heterodimerization. *Protein Eng.* **9**, 617–621 (1996).
10. Klein, C. *et al.* Progress in overcoming the chain association issue in bispecific heterodimeric IgG antibodies. *mAbs* **4**, 653–663 (2012).
11. Merchant, A.M. *et al.* An efficient route to human bispecific IgG. *Nat. Biotechnol.* **16**, 677–681 (1998).
12. Schaefer, W. *et al.* Immunoglobulin domain crossover as a generic approach for the production of bispecific IgG antibodies. *Proc. Natl. Acad. Sci. USA* **108**, 11187–11192 (2011).
13. Leaver-Fay, A., Jacak, R., Stranges, P.B. & Kuhlman, B. A generic program for multistate protein design. *PLoS ONE* **6**, e20937 (2011).
14. Havranek, J.J. & Harbury, P.B. Automated design of specificity in molecular recognition. *Nat. Struct. Biol.* **10**, 45–52 (2003).
15. Ashworth, J. *et al.* Computational redesign of endonuclease DNA binding and cleavage specificity. *Nature* **441**, 656–659 (2006).
16. Grigoryan, G., Reinke, A.W. & Keating, A.E. Design of protein-interaction specificity gives selective bZIP-binding peptides. *Nature* **458**, 859–864 (2009).
17. Tan, P.H., Sandmaier, B.M. & Stayton, P.S. Contributions of a highly conserved VH/VL hydrogen bonding interaction to scFv folding stability and refolding efficiency. *Biophys. J.* **75**, 1473–1482 (1998).
18. Igawa, T. *et al.* VH/VL interface engineering to promote selective expression and inhibit conformational isomerization of thrombopoietin receptor agonist single-chain diabody. *Protein Eng. Des. Sel.* **23**, 667–677 (2010).
19. De Groot, A.S. & Martin, W. Reducing risk, improving outcomes: bioengineering less immunogenic protein therapeutics. *Clin. Immunol.* **131**, 189–201 (2009).
20. Nahta, R., Hung, M.C. & Esteva, F.J. The HER-2-targeting antibodies trastuzumab and pertuzumab synergistically inhibit the survival of breast cancer cells. *Cancer Res.* **64**, 2343–2346 (2004).
21. Schmiedel, J., Blaukat, A., Li, S., Knochel, T. & Ferguson, K.M. Matuzumab binding to EGFR prevents the conformational rearrangement required for dimerization. *Cancer Cell* **13**, 365–373 (2008).
22. Ye, X. *et al.* An anti-Axl monoclonal antibody attenuates xenograft tumor growth and enhances the effect of multiple anticancer therapies. *Oncogene* **29**, 5254–5264 (2010).
23. Michaelson, J.S. *et al.* Anti-tumor activity of stability-engineered IgG-like bispecific antibodies targeting TRAIL-R2 and LTbetaR. *mAbs* **1**, 128–141 (2009).
24. Gunasekaran, K. *et al.* Enhancing antibody Fc heterodimer formation through electrostatic steering effects: applications to bispecific molecules and monovalent IgG. *J. Biol. Chem.* **285**, 19637–19646 (2010).
25. Garber, E. & Demarest, S.J. A broad range of Fab stabilities within a host of therapeutic IgGs. *Biochem. Biophys. Res. Commun.* **355**, 751–757 (2007).
26. Scheer, J.M. *et al.* Reorienting the Fab domains of trastuzumab results in potent HER2 activators. *PLoS ONE* **7**, e51817 (2012).
27. Li, B. *et al.* Bispecific antibody to ErbB2 overcomes trastuzumab resistance through comprehensive blockade of ErbB2 heterodimerization. *Cancer Res.* **73**, 6471–6483 (2013).
28. Feige, M.J. *et al.* An unfolded CH1 domain controls the assembly and secretion of IgG antibodies. *Mol. Cell* **34**, 569–579 (2009).

ONLINE METHODS

Computational design. The C_H1-Cλ interface was designed separately from the V_H-V_L interface. The 3TV3 IgG1-λ Fab structure[29] was selected as a starting model for C_H1-C_λ designs. Later modeling used our own crystal structures of intermediate designs as input. Residues appropriate for mutation at the C_H1-C_L interface were chosen with the assistance of Rosetta's InterfaceAnalyzer module[30]. 3TV3 was clipped to residues 106A–211 in chain L and 112–226 in chain H. We chose 37 positions (19 on C_L and 18 on C_H1) as mutable, based on the proximity of their side chains to the interface. Initial design at the V_H-V_L interface proceeded using PDB 3TCL[31] as a backbone. 3TCL was clipped to residues 1–113 in chain A and 1–107 in chain B. Twenty-one positions (10 in V_H and 11 in V_L) were chosen for mutation (**Supplementary Table 5**). All structures used as input for multistate design had their side chains pre-relaxed into the Rosetta score function using a global repacking operation. A command line is available as **Supplementary Protocol 1**.

Multistate design[13] was performed, allowing identified positions to mutate in various combinations. Using C_H1-Cλ as an example, we modeled as a positive state the mutant C_H1–mutant C_L pair and as negative states the mutant C_H1–WT C_L and WT C_H1–mutant C_L pairs. We forced the design simulations to mutate within clusters of proximal residues. Following fixed backbone sequence optimization, we reevaluated each design with a redocking protocol that allowed rigid-body motion between the two chains[30,32,33]. This docking analysis also explicitly models the three states (pairs) above. Manually selected back-mutations of initial sequence hits were computationally examined using the same docking algorithm, allowing us to reduce the number of mutations per design by removing mutations that made less important or more minor contributions to the specificity of pairing. In some experiments, we allowed only localized clusters to mutate. In other experiments, we allowed any of 37 positions to mutate, but inserted a term into the fitness function that penalized making more than a few mutations at once. In addition, some designs (**Supplementary Table 1**, paradigms 5 and 6) were selected by human inspection using the expert mode of FoldIt, a Rosetta-based protein simulator and confirmed using the same docking analysis[34]. The core mutations within CRD1, CRD2β and CRD2 were all found using local clusters of mutations. VRD2 was found using global interface design.

A mockup of the experimental setup used to generate the first design paradigm is presented as **Supplementary Protocol 2**. Rosetta's multistate design application[13] requires user specification to determine the experiment to be run. The fitness function used within multistate design is specified by the fitness.daf file present in **Supplementary Protocol 2**. Broadly, the fitness functions followed a similar form: the total energy and binding energy of the desired orthogonal heavy chain–light chain design interface was favored, the binding energy of the noncognate WT–design and design–WT heavy chain–light chain complexes was disfavored, and, on occasion, a final term proportional to the number of mutations disfavored mutation. The noncognate pair binding energies were clipped to a small negative value because bad clashes will produce falsely positive binding energies, which realistically would relax to weak-to-no interaction. The mutation term was also clipped to be zero in the presence of small numbers of mutations. All terms are independently premultiplied by separate weights. Choosing a fitness function is highly empirical, and many were tested over the course of the study.

Rosetta's multistate design uses a genetic algorithm to sample sequences rated by the fitness function[13]. However, the standard score12prime score function, which is insensitive to states, was used during design and packing[35]. As a result, the direct results of a single multistate design run were closely related, and multiple independent runs of multistate design (from the same setup) were necessary to widely sample sequence space and detect if diverse designs are plausible. This is unlike single-state design, in which all designs produced are independent. These experiments typically generated 10–1,000 independent multistate runs from a single setup.

A redocking protocol was used to verify designs. The protocol is described with a Rosetta command line in **Supplementary Protocol 3**. The single protocol represented here is one of many tested during the course of this study. This docking protocol and others were all used simultaneously and independently for those designs. The 3TCL crystal structure performs poorly in simple redocking using this protocol; accordingly the VRD2 mutations were selected without redocking.

Some mutations were found by means of rational design. In particular, the charge mutations in CRD1 (C_L_K129D, C_H1_D146K) were rationally selected based on the structure and subsequently tested for their viability using FoldIt[34]. It must be noted that this was done locally by one researcher using the "expert mode" that allows free modeling, not using the objective-oriented game mode, and in particular not using the crowdsourcing aspect of the application. The disulfide bond present between C_H1-C_L complexes is peripheral to the interface and was ignored during design and docking. Final models were all sufficiently close to native in rigid-body orientation that we expected the heavy chain–light chain disulfide to be preserved.

All mutants suggested by any design source were back-mutated to WT to identify the mutations most important to the design. In particular, the two mutations present in VRD2 were picked out of a background of many mutations suggested by multistate design. All manually selected back-mutations were reevaluated using the computational redocking protocol.

Final analysis of mutants was assisted with Rosetta's InterfaceAnalyzer tool[30]. The multistate fitness function can be reconstructed after redocking from the total and binding energies of the various desired and undesired complexes. For analysis at this level, we usually used a different fitness function that favored total and binding energy of the desired state, disfavored total and binding energy of the undesired state, and ignored the number of mutations. Designs with too many mutations were back-mutated rather than ranked differently.

Physical construction of test articles. To test the variable domain designs, we created a pertuzumab[36] human IgG1 with a human chimeric kappa V_L and lambda C_L (C_λ). Briefly, the pertuzumab V_H domain insert was generated with a PCR-based overlapping oligonucleotide synthesis procedure[37] using the sequence from the published crystal structure[36]. The insert contained appropriate AgeI and NheI restriction sites that enabled it to be ligated directly into a linearized modified pE vector (Lonza) containing an IgG1 constant domain sequence. The pertuzumab V_L gene was also generated using overlapping oligonucleotide synthesis. A DNA sequence encoding the V_L domain fused to C_λ was constructed using PCR and a modified plasmid template containing the C_λ sequence. Both 5′ and 3′ flanking oligonucleotides and two internal primers were designed to anneal the C terminus of the pertuzumab V_L domain to the N terminus of C_λ. The light chain insert was designed with HindIII and EcoRI restriction sites for direct ligation into a linearized modified pE vector (Lonza) with a selectable GS marker system. Each pE mammalian expression vector was engineered to contain a common mouse antibody light chain signal sequence that is translated in-frame as part of the expressed protein and cleaved before secretion. Constructs lacking variable domains or containing variable domains from other antibodies were subcloned into these heavy chain and light chain plasmids using standard cloning practices. All ligation constructs were used to transform *E. coli* strain TOP10 competent cells (Life Technologies). Transformed bacterial colonies were picked and cultured, and the plasmids were prepped. Correct sequences were confirmed by DNA sequencing.

For generating small sets of mutations, the QuikChange II Site Directed Mutagenesis Kit (Agilent) was used following the instructions provided by the manufacturer. For generating large sets of mutations (typically >3 mutations per chain), a gene synthesis strategy was employed (G-blocks, IDT). The synthesized genes were designed to be compatible with the heavy chain and light chain construct lacking variable domains. However, within the heavy chain construct, an Xho I site upstream of the common mouse light chain signal sequence was deleted using site-directed mutagenesis and a new Xho I site was generated at the C terminus (3′ end) of the coding region of the C_H1 domain. Synthesized genes were ligated to the heavy chain plasmid using the NheI and new XhoI restriction sites. Synthesized genes were added to the light chain plasmid using the BamHI and EcoRI restriction sites.

Expression and characterization of designed proteins. Each plasmid was scaled up by transformation into TOP10 *E. coli*, mixed with 100 ml Luria broth in a 250 ml baffled flask and shaken O/N at 220 r.p.m. Large-scale plasmid purifications were done using the BenchPro 2100 (Life Technologies) according to the manufacturer's instructions.

For protein production, plasmids harboring the heavy chain and light chain DNA sequences were transfected (1:2 plasmid ratio for the heavy chain and light chain plasmids, respectively) into HEK293F cells using Freestyle transfection reagents and protocols provided by the manufacturer (Life Technologies). Transfected cells were grown at 37 °C in a 5% CO_2 incubator while shaking at 125 r.p.m. for 5 d. Secreted protein was harvested by centrifugation at 10 K r.p.m. for 5 min. Supernatants were passed through 2 μm filters (both large scale and small scale) for purification. Small scale (1 ml) purifications were done by directly incubating 1 ml transfected supernatant with 100 μl resuspended, PBS-washed Protein G magnetic beads (Millipore). Beads were washed twice with PBS and once with PBS diluted tenfold. Protein was eluted from the beads by adding 130 μl 0.01 M Acetate, pH 3.0. After harvesting, the eluants were immediately neutralized by adding 20 μl 0.1 M Tris, pH 9.0.

Protein characterization by SDS-PAGE, analytical size-exclusion with in-line static light scattering (SEC-LS) and differential scanning calorimetry (DSC) was performed as described previously[38]. Enzyme-linked immunosorbent assays (ELISAs) were used to detect the amount of soluble IgG or IgG(–Fv) protein remaining after heat challenge for 1 h at elevated temperatures. For the pertuzumab protein, 96-well U-bottom high protein binding 96-well plates (Greiner bio-one) were coated overnight at 4 °C with 100 μl/well of a polyclonal anti-human C_λ antibody (Southern Biotech, cat#2070-01) at 2 μg/ml in a 0.05 M $NaHCO_3$ buffer, pH 8.3. The plates were then washed four times with PBS with 0.02% Tween80 (PBST) and blocked for 1 h with casein (Thermo) at 37 °C. The plates were washed again, followed by the addition of isolated HEK293F culture supernatants containing the pertuzumab IgG1-λ protein designs (100 μl/well). Aliquots of each supernatant were preexposed to various temperatures for 1 h using a PCR instrument with a 25 °C thermal gradient window. The thermally challenged pertuzumab IgG1-λ proteins (with or without mutations in the C_H1-C_L domains) were incubated on the plate for 1 h at 37 °C. The plates were then washed and 200 ng/ml in-house biotinylated human HER2-Fc (R&D systems, cat#1129-ER-050) was added at 100 μl/well (diluted in casein) for 1 h at 37 °C. The plates were washed again followed by the addition of streptavidin–horseradish peroxidase (HRP) (Jackson ImmunoResearch, cat#016-030-084) diluted 1:2,000 in casein. The plates were then washed and SureBlue Reserve TMB 1-component substrate (KPL) was added at 100 μl/well. The reaction was allowed to proceed for 5–15 min then quenched by the addition of 1% H_3PO_4. The absorbance at 450 nm was read using a SpectraMax 190 UV plate reader (Molecular Devices). A similar procedure was followed for the analysis of thermally challenged IgG1/λ proteins lacking variable regions. The only difference was that a sheep polyclonal anti-human C_H1 antibody (2 μg/ml in casein; Meridian Life Sciences, cat#W90075C) was used to capture proteins from the supernatants and an HRP-labeled polyclonal anti-human C_λ antibody (1:2,000 dilution in casein; Southern Biotech, cat#2070-05) was used for detection (replacing the HER2-Fc-biotin and streptavidin-HRP).

Affinity measurement of the mAbs and BsAbs. Affinities of the mAbs containing heavy chain–light chain redesigns were determined using surface plasmon resonance (Biacore 3000, GE Lifesciences). Fabs were generated from the WT pertuzumab IgG1 and VRD1_CRD2- and VRD2-containing IgG1s as described previously[39]. Goat anti-human IgG-Fc (Jackson Immunolabs, cat#109-005-098) was diluted to 40 μg/ml in 10 mM acetate, pH 5, and immobilized to a CM5 chip surface to ~10,000 RU using standard 1-ethyl-3-(3-dimethylaminopropyl)carbodiimide (EDC)/N-hydroxysuccinimide (NHS) amine coupling protocols. Human HER2-Fc (R&D systems, cat#1129-ER-050) at 20 nM was captured on the sensorship surface by injection for 4 min at 5 μl/min. The flow was increased to 30 μl/min and a secondary injection of each Fab (at 50, 35, 20, 10, 5, 2 or 1 nM) was performed. The running buffer (and dilution buffer) was HBS-EP 10 mM Hepes, 150 mM NaCl, 3 mM EDTA, 0.005% polysorbate 20. The chip surface was regenerated by two 10 s injections of 0.1 M glycine, pH 2.0. The concentration series were fit to a 1:1 binding model to determine the binding (k_a) and dissociation (k_d) rate constants and the equilibrium dissociation constant (K_D).

Dual-binding behavior of the BsAbs was also demonstrated by surface plasmon resonance. Human HER2-Fc and Axl-Fc (R&D Systems, cat#s 1129-ER-050 and 154-AL-100) were immobilized to CM5 chip surfaces as described above. Dual binding was demonstrated by injecting 20 nM HER2 × EGFR BsAb or cMetxAxl BsAb (300–540 s) over their appropriate chip surfaces followed by a 20 nM injection (920–1160 s) of human EGFR-Fc or cMet-Fc (R&D Systems, cat#s 344-ER-050 and 358-MT-100/CF) in HBS-EP buffer at 20 μl/min. Surfaces were regenerated using two 10 s injections of 0.1 M glycine, pH 2.0. Monovalent anti-HER2, anti-EGFR, anti-cMet and anti-Axl mAbs were injected as controls.

Mass spectrometric determination of light chain specificity and IgG BsAb assembly. Methods for liquid chromatographic purification of 2 ml mammalian cell culture samples and mass spectrometric analysis of purified proteins were presented at the 8th Symposium on the Practical Applications of Mass Spectrometry in the Biotechnology Industry (M.A. Batt, J.R. Fitchett, J.Y. Hannah, M. LaBarre and B.E. Jones, 2011. Intact mass analysis of protein G titer samples, Poster P-103) and a manuscript describing these methods is in preparation. Briefly, proteins were purified on an Agilent 1100 HPLC using a protein G (PG) ID sensor cartridge (Life Technologies). Purified samples were analyzed on an Agilent 6210 time-of-flight liquid chromatography/mass spectrometry (LC/MS) system molecular weight analyzer. Theoretical mass-averaged molecular weights of the light chain and heavy chain components were determined using the GPMaw program (v. 8.20). For the light chain competition experiments, the relative counts of the ionized light chains hitting the detector are used to quantify the ratio of designed versus WT light chain bound to a designed or WT heavy chain.

C_H1-C_L protein crystallization. To generate protein for crystallography, isolated C_H1-C_λ proteins (disulfide linked) were produced in *E. coli*. The isolated C_H1-C_λ proteins (which contained neither V regions nor an IgG-Fc) were subcloned into the pET-DUET plasmid from Novagen. The C_H1 insert (with a pelB signal sequence for secretion into the periplasmic space) was synthesized (with a hexahistidine C-terminal tag) using overlapping PCR[37] and subcloned into cassette 1 of the plasmid using the NheI and BamHI sites. The C_λ insert was similarly synthesized and inserted between the NdeI and XhoI sites. Designs CRD1 and CRD2β were generated from this WT plasmid using QuikChange II mutagenesis (Agilent). Each plasmid was transformed into CodonPlus BL21(DE3) chemically competent cells (Agilent) for expression. For each protein preparation, transformed and pre-cultured cells were used to inoculate 2X1.4 l Luria broth supplemented with 100 μg/ml carbenicillin and 35 μg/ml chloramphenicol. The cultures were allowed to shake at 220 r.p.m. at 37 °C until the OD_{600} reached 1–1.5. At this stage, the culture temperature was reduced to 30 °C and 1 mM isopropyl-1-thio-β-D-galactopyranoside was added. The cultures were allowed to grow for 3–4 h and harvested by centrifugation for 20 min at 4,000*g*. The proteins were resuspended in 50 ml of a periplasmic extraction buffer (500 mM sucrose, 100 mM Tris, pH 8, 1 mM EDTA and 100 μg/ml hen-egg white lysozyme). The extracted proteins were diluted tenfold into a 10 mM citrate, 10 mM NaCl buffer, pH 5.5, and passed over a 5 ml SP Sepharose FF HiTrap cation exchange column (GE Healthcare) at 5 ml/min using an AKTA Explorer (GE Healthcare). The proteins were eluted from the column using a gradient up to 0.7 M NaCl. The proteins were dialyzed into PBS and captured onto a Ni-Sepharose HiTrap affinity column. The proteins were eluted using a gradient up to 0.3 M imidazole. The proteins were concentrated to ~3–10 mg/ml and filtered.

For crystallography, the WT C_H1-C_L protein was screened using the vapor diffusion crystallization method, whereby protein is first mixed with well solution and deposited in a small chamber with well solution, sealed and allowed to equilibrate with well solution, concentrating both protein and precipitating reagents in the protein drop. Crystallization trials were conducted in a 96-well format (Intelli-plates, Art Robins Instrument) using the commercially available screens: PEGs, PEGs II, ComPAS, Classics and Classics II Suites (Qiagen). A Phoenix robot (Art Robins Instrument) deposited 0.3 μl of protein on 0.3 μl of well solution. Crystallization occurred in 30% PEG4K at 21 °C. Crystals grew to full size within 3 d. Crystals were transferred to a cryo-protection solution of the reservoir solution with 40% PEG4K and 20% PEG400 and flash frozen by immersion in liquid nitrogen before shipping to the Advanced Photon Source for data collection. The C_H1-C_L protein with CRD1 was similarly screened and streak-seeded using WT C_H1-C_L crystal seeds. Crystals were grown at 21 °C by mixing 1.2 μl of 3.9 mg/ml protein and 1.2 μl of reservoir solution, containing 40% PEG6K and 10 mM tri-sodium citrate dehydrate. Crystals were cryo-protected using reservoir solution increased

doi:10.1038/nbt.2797

by 50% PEG6K and 20% ethylene glycol. The C_H1-C_L protein with CRD2β crystallized directly in conditions developed for CRD1. Single crystals were grown at 21 °C by mixing 1.5 µl protein with 1.5 µl of reservoir, containing 39% PEG 6K and 10 mM tri-sodium citrate. Crystals were cryoprotected using the same technique as for CRD1.

Fab protein crystallization. Fab proteins were produced by proteolytic cleavage of the full-length IgGs using papain as described previously[39]. Pertuzumab Fab (with Cλ) crystal screening was performed at 16 mg/ml protein. Crystals could be obtained only by heterogeneous cross-seeding with crystals of an IgG4 Fc protein (in-house protein). The crystals (thin microcrystalline plates) appeared after 4 d in 100 mM sodium acetate pH 4.6/30% PEG MME 2K/200 mM ammonium sulfate. Optimization was done as described above except the pH of sodium acetate buffer was also varied. Optimization produced thin intergrown plates, grown in sitting drops by mixing 1.5 µl of protein with 1.5 µl of reservoir solution, containing 100 mM sodium acetate buffer pH 4.4/31% PEG MME 2K/200 mM ammonium sulfate. Crystals were cryo-protected in reservoir solution with PEG MME 2K. Concentration was increased by 10% and supplemented with 20% glycerol. Improved order within the variable domains was achieved by generating crystal in the same conditions, plus 10% MPD at 12.4 mg/ml protein. The pertuzumab Fab containing VRD2 was crystallized using 15 mg/ml protein. The drops were streak-seeded with WT pertuzumab crystals seeds. Plate-shaped crystals appeared within a week and grew to their full size within an additional 3 d at the following conditions: 15% PEG 8K/200 mM ammonium sulfate. The pertuzumab Fab containing VRD1_CRD2 was initially crystallized using 14.3 mg/ml protein after 5 d in the PEG Rx HT screen using 100 mM sodium citrate pH 5/30% Jeffamine ED-2001 pH 7 (Hampton Research). Crystals diffracting at higher resolution were obtained by seeding using the PEG Rx HT crystals and incubation in the PEG RC HT crystal screen reagent C1 with 100 mM sodium citrate pH + 30% Jeffamine ED-2001 pH 7 for 5 d. Crystals were transferred to a cryo-protection solution of the reservoir solution with PEG8K increased by 10% and supplemented by 20% ethylene glycol and flash frozen by immersion in liquid nitrogen before shipping to the Advanced Photon Source for data collection.

Structure determination. X-ray diffraction data were collected under standard cryogenic conditions at the Advanced Photon Source (Argonne National Laboratory) using the LRL-CAT beamline and reduced to structure factor amplitudes using MOSFLM, SCALA and TRUNCATE[40,41]. All structures were solved using PHASER[42], refined using REFMAC[43], and visualized and rebuilt using XTALVIEW/XFIT[44]. The WT C_H1:C_λ structure was solved using the program Phaser with the C_H1 and C_λ domains of PDB 3THM as search models. Structures of subsequent design mutants (CRD1 and an intermediate of CRD2) were solved by Phaser using this parent structure as a search model. The parent Fab, pertuzumab with C_λ, was solved using the in-house C_H1:C_λ structure and the variable domains of pertuzumab (PDB: 1S78). The stereochemical quality of the atomic model was monitored using an automated quality control procedure. **Supplementary Table 4** provides data collection and crystallographic statistics for the fully refined structures.

Cytotoxicity assays. PBMCs were ordered from SeraCare. They were thawed and aliquoted into 24-well plates (1 M cells per well) or into a T75 flask depending on cell number. Prior to adding the PBMCs to the plates, each well or flask was coated overnight at 4 °C with the anti-CD3 mAb BDACHT1 (BD Biosciences) at 5 µg/ml in PBS. Anti-CD28 (2.5 µg/ml, BD Biosciences, cat#556620), hIL-2 (5 ng/ml R&D Systems, cat#202-IL-010), 10% FBS (Corning), gentamicin (50 µg/ml Gibco) and L-glutamine (200 mM, Gibco) were added to the RPMI media (MediaTech) used to expand the PMBCs. Fresh media lacking the anti-CD28 mAb but containing hIL-2 was added again at day 3. The PBMCs were cultured for at least 4 d before being used for redirected cell lysis.

A431 and BT474 cells were purchased from the American Type Culture Collection (ATCC). All tumor cell lines here and in the sections below tested negative for mycoplasma in our laboratory. Each cell line was thawed and aliquoted into T75 flasks and expanded in RPMI with 10% FBS. The adherent cells were detached from the plastic flasks with Accutase (Life Technologies) and labeled with BATDA chelate (DELFIA EuTDA Cytotoxicity Kit, PerkinElmer) according to the manufacturers' protocol. The tumor cells and the T cells (the latter were the effector cells) were then mixed at various tumor/effector cell ratios. The ratio chosen for this study was 1:25. Supernatants were isolated at various time points in the presence or absence of effector cells to provide an indicator of the extent of spontaneous versus effector-mediated BATDA release. Maximum release is determined by lysing the cells with the lysis buffer provided in the kit.

Western blot analysis. A549 NSCLC cells (ATCC; in-house tested as mycoplasma negative) were treated with control IgG1, cMet bivalent mAb, matuzumab, the cMet/matuzumab combination or the cMet × EGFR IgG for 1 h at 37 °C followed by a 15 min period where the cells were either stimulated with 0.1 µg/ml of EGF (R&D Systems, cat#236-EG-200) and HGF (generated recombinantly in-house) or not stimulated. Cellular proteins were extracted in a cell lysis buffer (Cell Signaling Technology) and protein concentrations in lysates were measured using the colorimetric BCA protein assay kit (Pierce Protein Research Products). Equal amounts of protein were separated on a NuPage 4–12% Tris-Bis gel (Life Technologies) and transferred to a nitrocellulose membrane (0.45 µm pore). The blots were probed with primary mAbs (all from Cell Signaling Technology) specific for phospho-cMet (Tyr1234), phospho-EGFR(Tyr1173, cat#4407), total cMet (cat#8198) and total EGFR (cat#2232); they were then probed with a secondary conjugate anti-rabbit-IgG-HRP (Jackson ImmunoResearch Laboratories, cat#111-035-003) followed by development with Supersignal Western Substrate Kit (Pierce Protein Research Products). For detecting Actin, a primary mouse anti-beta Actin mAb (Sigma, cat#A2228) followed by goat anti-mouse IgG-HRP (Cell Signaling Technologies, cat#7076) was used. Chemiluminescence images were captured using a UVP imaging system.

Mesoscale discovery. Phospho-cMet and total cMet levels in cell lysates were measured using a MULTI-SPOT Phospho (Tyr1349)/Total Met MSD kit (Meso Scale Discovery). Plates were loaded with 25 µl/well of cell lysate and incubated at room temperature with vigorous shaking (300–1,000 r.p.m.) for 1 h and processed according to the manufacturer's protocol. Plates were read on the Sector Imager 2400 (Meso Scale Discovery). The percentage of phospho-protein over total protein was calculated using multiplex assay format: anti-total and anti-phospho-assay in the same well: % phosphoprotein = ((2 × phospho-signal)/(phospho-signal + total signal)) × 100.

Cell proliferation. NCI-N87 (gastric cancer, ATCC; tested in-house as mycoplasma negative) cells were seeded on 96-well plates at 1×10^3 cells per well and pre-cultured in RPMI-1640 medium containing 10% FBS overnight. To evaluate the impact of trastuzumab, pertuzumab, the mAb combination and the $HER2^P \times HER2^T$ IgG BsAb on cell proliferation, 300, 30, 3 and 0.3 nM solutions of each test article (or combinations of 300, 30, 3 and 0.3 nM of each test article) in RPMI-1640 medium containing 10% FBS were added to the cells. After 5 d treatment, cell viability was determined with a Cell Titer Glo reagent (Promega). The percentage of growth inhibition was calculated according to the formula (1-(signal with mAb (or BsAb))/(signal with FBS only))*100. Values between different measurements were individually compared using an unpaired *t*-test where normal distribution and equal variance parameters were met.

Pharmacokinetics. All animal studies were conducted under Institutional Animal Care and Use Committee–approved protocols and within an Association for Assessment and Accreditation of Laboratory Animal Care International (AAALAC)-accredited facility. Male BALB/c mice (7–8 weeks old; Harlan Laboratories, Indiana, USA) were injected intravenously with a single bolus (~150 µl) of 10 mg/kg of mAb or BsAb on day 0. Mice were randomized based on body weight and doses were adjusted accordingly to match body weight. Blood samples were collected through the retro-orbital plexus using heparinized capillary tubes at various time points ($n = 4$ per time point; no statistical methods were used to predetermine sample size) and plasma samples were isolated for subsequent mAb or BsAb quantification by ELISA. Investigators were not blinded to the identity of samples from the different animal groups.

For quantification of the parental mAbs in serum, ELISAs were carried out by coating a High Bind U-well 96-well plate (Greiner Microlon) with

2 μg/ml antigen in 50 mM sodium carbonate, pH 9.3 overnight at 4 °C, washing with PBS+0.1%, Tween20 (PBST), blocking for 1 h with casein at room temperature (RT), washing with PBST, adding plasma diluents starting at 1:50 in PBST for 1 h at RT, washing with PBST and adding a 1:1,000 diluted goat anti-human-Fc-AP polyclonal (Southern Biotech) in PBST with 1% BSA for 1 h at room temp. The detection reagent was washed off followed by the addition of PNPP Substrate (Thermo Scientific). Colorimetric readout was performed on a SpectraMax 190 plate reader. For the BsAbs, the first antigen was coated on the plate and bound BsAb was detected using a biotinylated 2nd antigen to ensure that bispecific activity was maintained. The biotinylated detection antigen was detected using a secondary step with streptavidin-AP (Jackson ImmunoResearch).

Data sets were subjected to outlier analysis using the ROUT method (GraphPad Prism, California, USA) before pharmacokinetic parameter determination. For each mAb or BsAb the average plasma concentrations in μg/ml versus time were fitted to an IV-bolus two-compartment model or by noncompartmental analysis (MetMAb only) using Phoenix Winnonlin modeling software (Pharsight Co., Virginia, USA). Pharmacokinetic parameters determined included: t 1/2 β, elimination half-life; AUC, area under the curve; CL, clearance; Vss, volume of distribution at steady state.

29. Pejchal, R. *et al*. A potent and broad neutralizing antibody recognizes and penetrates the HIV glycan shield. *Science* **334**, 1097–1103 (2011).
30. Lewis, S.M. & Kuhlman, B.A. Anchored design of protein-protein interfaces. *PLoS ONE* **6**, e20872 (2011).
31. McLellan, J.S. *et al*. Structure of HIV-1 gp120 V1/*V2* domain with broadly neutralizing antibody PG9. *Nature* **480**, 336–343 (2011).
32. Gray, J.J. *et al*. Protein-protein docking with simultaneous optimization of rigid-body displacement and side-chain conformations. *J. Mol. Biol.* **331**, 281–299 (2003).
33. Fleishman, S.J. *et al*. RosettaScripts: a scripting language interface to the Rosetta macromolecular modeling suite. *PLoS ONE* **6**, e20161 (2011).
34. Cooper, S. *et al*. Predicting protein structures with a multiplayer online game. *Nature* **466**, 756–760 (2010).
35. Leaver-Fay, A. *et al*. Scientific benchmarks for guiding macromolecular energy function improvement. *Methods Enzymol.* **523**, 109–143 (2013).
36. Franklin, M.C. *et al*. Insights into ErbB signaling from the structure of the ErbB2-pertuzumab complex. *Cancer Cell* **5**, 317–328 (2004).
37. Casimiro, D.R., Wright, P.E. & Dyson, H.J. PCR-based gene synthesis and protein NMR spectroscopy. *Structure* **5**, 1407–1412 (1997).
38. Dong, J. *et al*. Stable IgG-like bispecific antibodies directed toward the type I insulin-like growth factor receptor demonstrate enhanced ligand blockade and anti-tumor activity. *J. Biol. Chem.* **286**, 4703–4717 (2011).
39. Doern, A. *et al*. Characterization of inhibitory anti-insulin-like growth factor receptor antibodies with different epitope specificity and ligand-blocking properties: implications for mechanism of action in vivo. *J. Biol. Chem.* **284**, 10254–10267 (2009).
40. Powell, H.R. The Rossmann Fourier autoindexing algorithm in MOSFLM. *Acta Crystallogr. D Biol. Crystallogr.* **55**, 1690–1695 (1999).
41. Evans, P.R. An introduction to data reduction: space-group determination, scaling and intensity statistics. *Acta Crystallogr. D Biol. Crystallogr.* **67**, 282–292 (2011).
42. McCoy, A.J. *et al*. Phaser crystallographic software. *J. Appl. Crystallogr.* **40**, 658–674 (2007).
43. Murshudov, G.N., Vagin, A.A. & Dodson, E.J. Refinement of macromolecular structures by the maximum-likelihood method. *Acta Crystallogr. D Biol. Crystallogr.* **53**, 240–255 (1997).
44. McRee, D.E. XtalView/Xfit–A versatile program for manipulating atomic coordinates and electron density. *J. Struct. Biol.* **125**, 156–165 (1999).

doi:10.1038/nbt.2797